Molecular Therapy
Original Article

Systemic AAV-Mediated β-Sarcoglycan Delivery Targeting Cardiac and Skeletal Muscle Ameliorates Histological and Functional Deficits in LGMD2E Mice

Eric R. Pozsgai,[1,2] Danielle A. Griffin,[2] Kristin N. Heller,[2] Jerry R. Mendell,[1,2,3] and Louise R. Rodino-Klapac[1,2,3]

[1]Biomedical Sciences Graduate Program, The Ohio State University, Columbus, OH 43210, USA; [2]Center for Gene Therapy, The Research Institute at Nationwide Children's Hospital, Columbus, OH 43205, USA; [3]Department of Pediatrics and Neurology, The Ohio State University, Columbus, OH 43210, USA

Limb-girdle muscular dystrophy type 2E (LGMD2E), resulting from mutations in β-sarcoglycan (*SGCB*), is a progressive dystrophy with deteriorating muscle function, respiratory failure, and cardiomyopathy in 50% or more of LGMD2E patients. *SGCB* knockout mice share many of the phenotypic deficiencies of LGMD2E patients. To investigate systemic *SGCB* gene transfer to treat skeletal and cardiac muscle deficits, we designed a self-complementary AAVrh74 vector containing a codon-optimized human *SGCB* transgene driven by a muscle-specific promoter. We delivered scAAV.MHCK7.hSGCB through the tail vein of SGCB$^{-/-}$ mice to provide a rationale for a clinical trial that would lead to clinically meaningful results. This led to 98.1% transgene expression across all muscles that was accompanied by improvements in histopathology. Serum creatine kinase (CK) levels were reduced following treatment by 85.5%. Diaphragm force production increased by 94.4%, kyphoscoliosis of the spine was significantly reduced by 48.1%, overall ambulation increased by 57%, and vertical rearing increased dramatically by 132% following treatment. Importantly, no adverse effects were seen in muscle of wild-type mice injected systemically with scAAV.hSGCB. In this well-defined model of LGMD2E, we have demonstrated the efficacy and safety of systemic scAAV.hSGCB delivery, and these findings have established a path for clinically beneficial AAV-mediated gene therapy for LGMD2E.

INTRODUCTION

The limb-girdle muscular dystrophies (LGMDs) are one major class of genetic disorders affecting the musculoskeletal system and the corresponding molecular components and processes. LGMD2E represents one of the most severe LGMDs, with worldwide reports of incidence of 1 in 200,000 to 1 in 350,000.[1] In this disease, mutations in the β-sarcoglycan (*SGCB*) gene lead to loss of functional protein with concurrent loss of other structural components of the sarcolemma-stabilizing dystrophin-associated protein complex (DAPC).[2,3] The result is a progressive decline in muscle function because of necrotic muscle fiber loss, enhanced inflammatory infiltration, and development of fibrotic tissue.[4,5]

LGMD type 2E (LGMD2E) patients exhibit typical but often more severe characteristics of LGMD, with widespread progressive muscle wasting, initial pelvic and shoulder girdle weakness, degrees of proximal muscle weakness, and evidence of Gower's maneuvers.[2,6–8] The spectrum of clinical presentation is heterogeneous; however, in the more severe Duchenne muscular dystrophy (DMD)-like cases, symptoms commonly start in early childhood, with increasing difficulty in mobility and eventual loss of ambulation in the second decade of life.[2,6–8] Because of extensive musculoskeletal involvement, reports of dystrophic mice and LGMD2E patients also indicate joint contractures and kyphoscoliosis (curvature) of the thoracic spine, which, when combined with the degenerating diaphragm, lead to compromised diaphragm and lung function.[8–12] Perhaps most compelling is that evolving studies have reported cardiac involvement in approximately 50% or more of LGMD2E cases. Cardiac dysfunction manifests in the form of cardiomyopathy (often dilated), resulting in impaired left and right ventricle function, heart rhythm abnormalities, and eventual myocardial hypertrophic remodeling.[8,13–16] Importantly, when considering a clinically effective therapy for patients, it is critical that the significant cardiac involvement, often a key morbidity factor in LGMD2E, be a major target of any therapeutic intervention.

The *sgcb*$^{-/-}$ murine model of LGMD2E, completely absent of β-sarcoglycan protein, displays a severe dystrophic phenotype that worsens with age, with frequent development of cardiomyopathy.[5] We and others have noted the severity of a histopathological hallmark of the *scgb*$^{-/-}$ mouse, fibrosis, evident by increased deposition of collagens and other extracellular matrix components.[5,17,18] Dystrophic histopathology in the myocardium and the development of cardiomyopathy have also been reported, with aged mice showing similar cardiac deficits as seen in LGMD2E patients.[4,5,19] The recapitulation of the LGMD2E disease phenotype in *sgcb*$^{-/-}$ mice provides an ideal

Received 24 October 2016; accepted 10 February 2017;
http://dx.doi.org/10.1016/j.ymthe.2017.02.013.

Correspondence: Louise R. Rodino-Klapac, Center for Gene Therapy, The Research Institute at Nationwide Children's Hospital, Room 3016, 700 Childrens Dr., Columbus, OH 43205, USA.
E-mail: louise.rodino-klapac@nationwidechildrens.org

model to study disease mechanisms and therapeutic development for patients. With virus-mediated gene replacement therapy emerging as a potential treatment for these diseases, we previously reported construction of a self-complementary adeno-associated viral vector (scAAV)[20,21] carrying full-length β-sarcoglycan cDNA driven by a muscle-specific promoter (triple muscle creatine kinase [tMCK]).[18] This was packaged into an AAVrh.74 virus, proven in mice and non-human primates to be safe and highly efficient in transducing muscle across the vascular barrier from the circulation.[22–24]

Following the completion of local and regional gene delivery with this transgene cassette,[18] we chose to alter our cassette to include the MHCK7 promoter, which expresses well in heart and skeletal muscle (including the diaphragm),[25] and use a systemic (intravenous) delivery approach to achieve correction of the skeletal and cardiac dysfunction in this disease. We demonstrate in this report the efficacy of a systemic delivery of our scAAV.rh.74.MHCK7.hSGCB vector with no adverse effects in treated mice. Along with nearly complete transduction of skeletal and cardiac muscle, we report functional restoration in diaphragm muscle, partial improvement in cardiac functional parameters, and significantly increased activity in vector-dosed mice. With no current cure or treatment for LGMD2E,[26] systemic (intravenous) delivery has become a primary goal, allowing for a comprehensive therapy for this disease. This has allowed clinical trials to progress past expectations of only safety and provides optimism for efficacy. As a result of the high incidence of cardiomyopathy in LGMD2E, we feel strongly that treatment of the heart in addition to skeletal muscle is vital for maximum long-term treatment, and these pre-clinical studies with a vector optimized for systemic therapy provide clear evidence for translation to LGMD2E patients.

RESULTS

scAAVrh.74.MHCK7.hSGCB Construction and Vector Potency

Our new therapeutic scAAVrh.74.MHCK7.hSGCB transgene cassette was constructed by replacing the tMCK promoter from our previously investigated vector[18] with the MHCK7 promoter to achieve enhanced cardiac expression[25] (Figure 1A). Viral potency in muscle was established by intravenous injection into the tail vein of *Sgcb* null mice at a dose of 1×10^{12} vector genome (vg) total dose (5×10^{13} vg/kg based on a 20-g mouse), followed by immunofluorescence analysis of muscles 1 month after gene transfer. The amount of hSGCB transgene expression in five different limb skeletal muscles, tibialis anterior (TA), gastrocnemius (GAS), quadriceps (QUAD), psoas major (PSOAS), and triceps (TRI), from both the left and right sides of the mice was quantified along with the diaphragm. A qualitative analysis of heart tissue was also used to assess the relative level of transgene expression in cardiac muscle upon delivery. Mice deficient for β-sarcoglycan were completely absent of the protein when analyzed by immunofluorescence. Our therapeutic dose of 1×10^{12} vg total dose resulted in a mean 97.96% ± 0.36% vector transduction across all skeletal muscles, including the diaphragm, and approximately 95% or greater in cardiac muscle (data not shown).

Long-Term Systemic Delivery of scAAVrh.74.MHCK7.hSGCB in SGCB$^{-/-}$ Mice

To build upon the results of the 1-month potency assay, we investigated longer-term (6-month duration) systemic delivery of the β-sarcoglycan transgene cassette to *sgcb*$^{-/-}$ mice. Four- to-five-week-old *sgcb*$^{-/-}$ mice were treated with a 1×10^{12} vg total dose of scAAVrh.74.MHCK7.hSGCB intravenously in the tail vein. Mice were necropsied 6 months post-injection, and hSGCB transgene expression was demonstrated using immunofluorescence in six skeletal muscles, both left and right, in addition to the diaphragm and heart of all treated mice. Skeletal muscles analyzed included TA, GAS, QUAD, gluteal (GLUT), PSOAS, and TRI. The mean hSGCB expression resulting from systemic delivery in treated mice was 98.13% ± 0.31% across all skeletal muscles, including the diaphragm, with expression in the heart exceeding >95%. Representative images are shown in Figure 1B. The expression levels in each individual muscle type averaged from all treated mice are shown in Table S1, and western blotting (Figure 1C) confirmed transgene expression in all muscles. Quantification of hSGCB transgene expression in hearts from treated mice via western blotting and densitometry indicate overexpression of hSGCB up to 72.0% above BL6 wild-type (WT) levels of expression (Figure 1D), correlating to the high levels quantified in skeletal muscle. We also assessed the restoration of additional DAPC components in cardiomyocytes following hSGCB gene transfer and found complete restoration of α-sarcoglycan and dystrophin expression (Figure S1).

An important characteristic of *sgcb*$^{-/-}$ muscle described in previous reports[4,5] and illustrated by the H&E staining of the GAS and diaphragm shown in Figure 2A is severe dystrophic pathology, including central nucleation (CN), necrosis, inflammatory infiltration, and fibrosis. Gene transfer significantly improves this pathology, alleviating many of these dystrophic features (Figure 2A). Quantification of histological parameters shows a significant reduction in CN in the various skeletal muscles analyzed above as a result of gene transfer (Figure 2B). With the expected low levels of CN in BL6 WT mice across all muscles averaging 1.89% ± 0.39%, we note here, taking into account all muscles analyzed, a mean of 66.85% ± 1.86% CN in untreated *sgcb*$^{-/-}$ mice compared with 36.30% ± 5.16% in AAV.MHCK7.hSGCB-treated *sgcb*$^{-/-}$ muscle ($p < 0.0001$) (Table S2). Further examination of central nucleation levels in several muscles demonstrates that hSGCB expression conferred complete protection from degeneration, given that the percent of CN fibers following 6 months of treatment was equivalent to levels seen in untreated *sgcb*$^{-/-}$ mice at the age of treatment of 4–5 weeks of age. Levels in treated *sgcb*$^{-/-}$ mice at 7 months of age compared with untreated *sgcb*$^{-/-}$ mice at 4–5 weeks of age were 43.85% ± 3.89% compared with 42.07% ± 16.25% in the TA muscle (no significance [ns]), 38.71% ± 3.50% compared with 28.16% ± 10.73% in the GAS muscle (ns), and 11.59% ± 2.08% compared with 36.88% ± 5.92% in the diaphragm ($p < 0.001$).

A more in-depth analysis of muscle histopathology reveals a normalization of fiber size distribution accompanied by an increase in mean fiber diameter in diseased mice treated with vector compared with

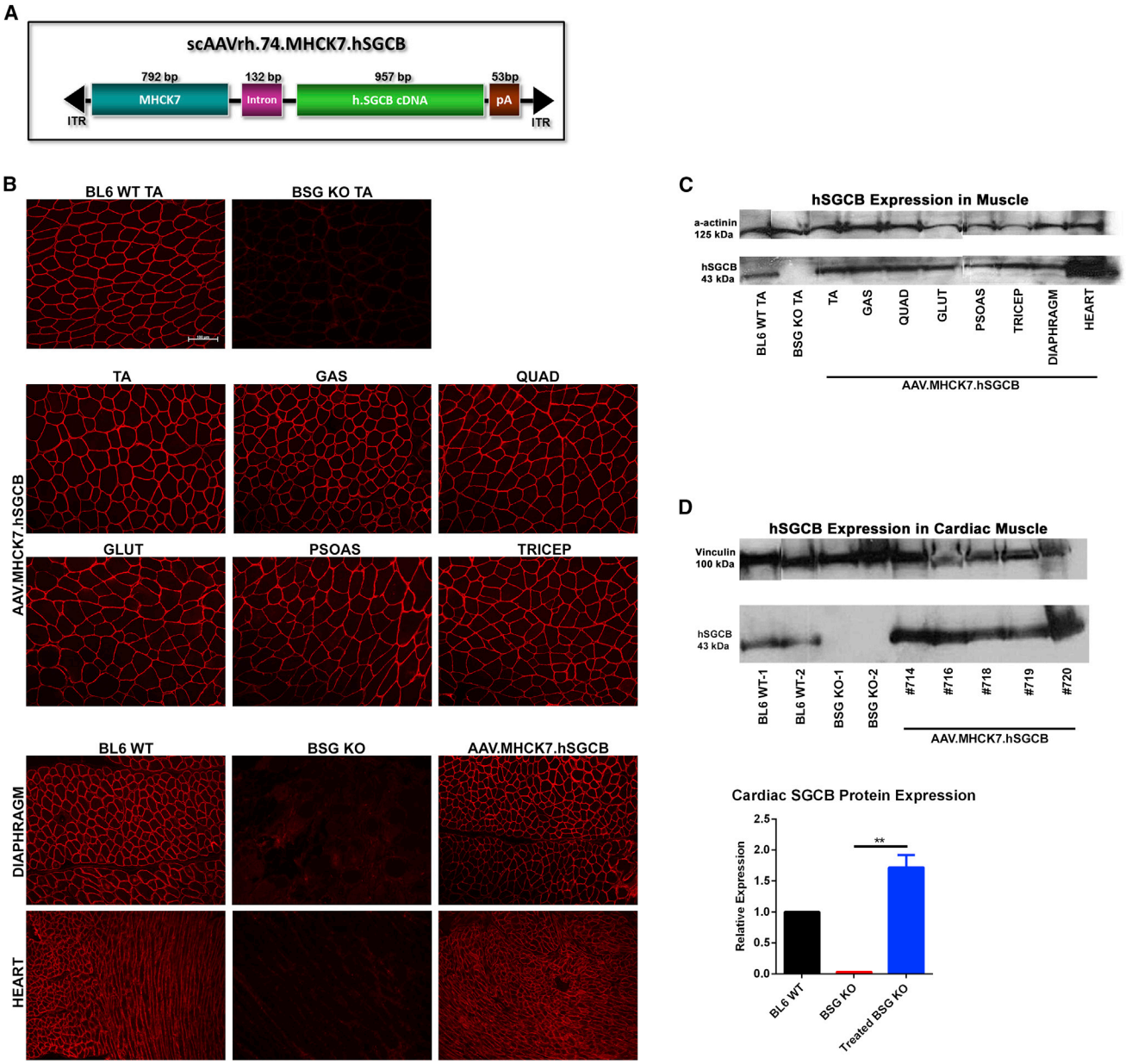

Figure 1. Restoration of SGCB Expression following Intravenous Delivery of scAAVrh.74.MHCK7.hSGCB

(A) scAAVrh.74.MHCK7.hSGCB cassette identical to our original cassette with the exception of the inclusion of the MHCK7 promoter instead of tMCK for expression in cardiac muscle. (B) Immunofluorescence imaging 6 months post-injection of skeletal muscles, diaphragm, and heart from sgcb$^{-/-}$ mice intravenously injected with a 1e−12 vg total dose of scAAVrh.74.MHCK7.hSGCB. Shown are representative images of skeletal muscles displaying a mean of 98.13% ± 0.31% transduction. Also shown are representative images of heart tissue displaying high levels of hSGCB transgene expression. 20× images are shown for all immunofluorescence (IF) images. Scale bar, 100 μm. (C) Western blotting of all muscles from one treated sgcb$^{-/-}$ mouse confirming hSGCB transgene expression. (D) Western blotting for hSGCB expression in the hearts of five sgcb$^{-/-}$ treated mice, with densitometry quantification showing overexpression of hSGCB up to 72.0% of BL6 WT levels.

untreated *sgcb*$^{-/-}$ mice in all three muscles examined (GAS: *sgcb*$^{-/-}$ untreated, 28.37 ± 0.23 μm versus AAV.hSGCB treated – 36.04 ± 0.17 μm; $p < 0.0001$) (PSOAS: sgcb−/− untreated – 24.75 ± 0.23 μm versus AAV.hSGCB-treated, 38.43 ± 0.28 μm, $p < 0.0001$; TRI: *sgcb*$^{-/-}$ untreated, 28 ± 0.31 μm versus AAV.hSGCB-treated, 35.56 ± 0.22 μm, $p < 0.0001$) (Figures 2C and 2D; Table S2). As a result of the degeneration and regeneration processes that occur during disease progression, high levels of CK activity can be seen in the sera of LGMD2E patients and mice. In accordance with this, we detected a significant increase in CK levels in untreated *sgcb*$^{-/-}$ mice

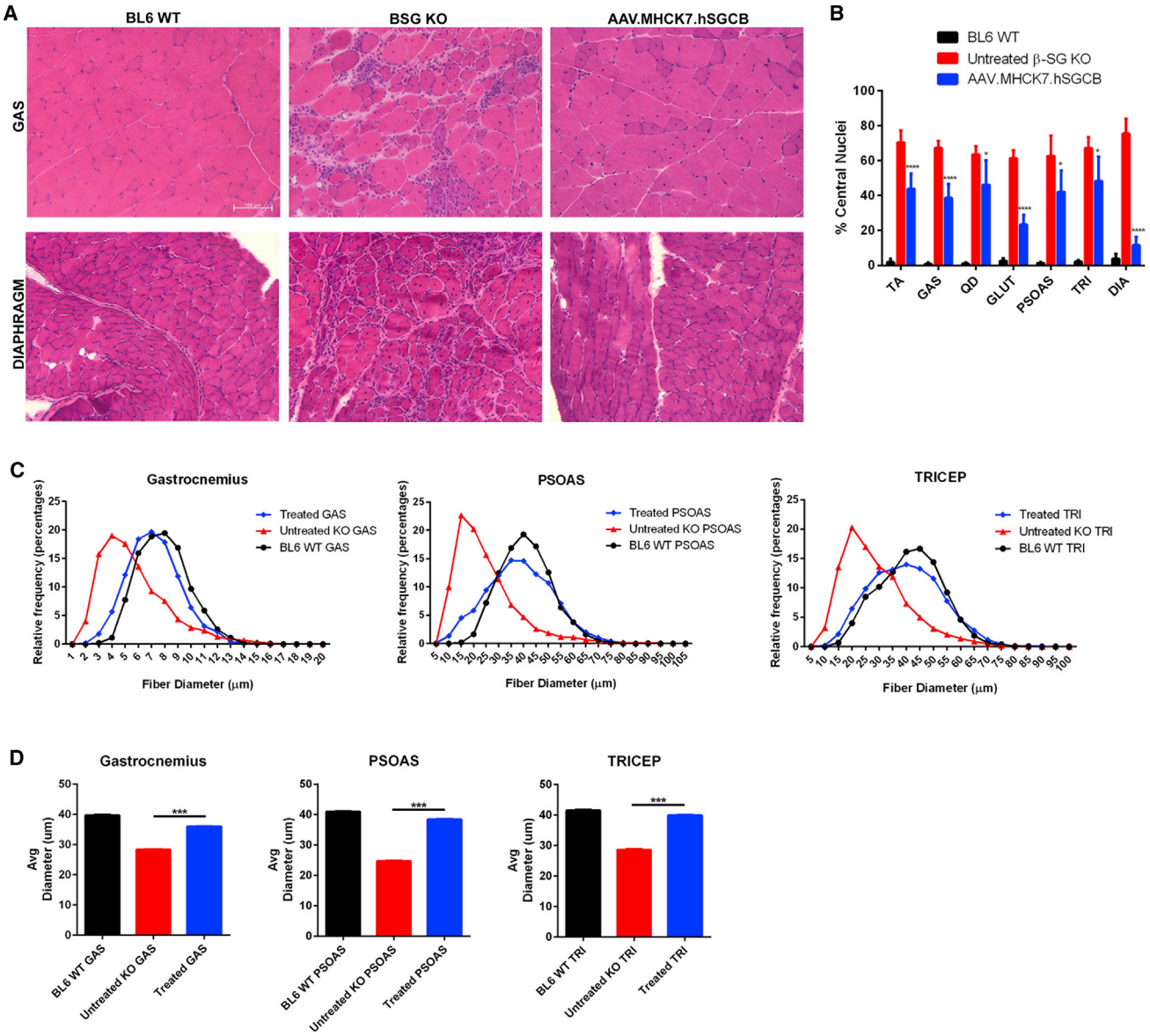

Figure 2. Effect of Systemic Treatment with scAAVrh74.MHCK7.hSGCB on Muscle Pathology

(A) H&E stain of diaphragm and QUAD muscle from C57BL/6 WT, *sgcb*$^{-/-}$, and scAAVrh.74.MHCK7.hSGCB-treated mice showing normalized histopathology. Representative 20× images are shown. Scale bar, 100 μm. (B) Quantification of reduction in centrally nucleated fibers in *sgcb*$^{-/-}$ treated muscle compared with untreated *sgcb*$^{-/-}$ muscle (TA, GAS, GLUT, and diaphragm, $p < 0.0001$; QUAD, PSOAS, and TRI, $p < 0.05$). (C and D) Normalization of fiber distribution in GAS, PSOAS, and TRI (C) and increase in mean fiber size in treated muscles compared to untreated *sgcb*$^{-/-}$ muscles (D) ($p < 0.001$, (n = 5/group).

at the endpoint age of 7 months (3667.0 ± 112.6 U/L) compared with BL6 WT mice at that age (43.89 ± 21.36 U/L) ($p < 0.0001$). Following systemic treatment with scAAVrh.74.MHCK7.hSGCB for 6 months, CK levels were decreased significantly compared with untreated *sgcb*$^{-/-}$ levels to 530.40 ± 103.8 U/L ($p < 0.0001$) (Figure S2).

Because of the significant role fibrosis plays in the pathogenesis of LGMD2E and effectiveness of therapies, it was critical to demonstrate the same efficacy in reducing fibrosis we saw with localized β-sarcoglycan gene transfer,[18] now following systemic delivery of scAAVrh.74.MHCK7.hSGCB. Using the picrosirius red stain for collagen types I and III, we analyzed the levels of collagen in the GAS and diaphragm muscles of 7-month-old BL6 WT mice, untreated *sgcb*$^{-/-}$ mice, and treated *sgcb*$^{-/-}$ mice 6 months post-injection. Treated muscles displayed significantly less collagen deposition compared with untreated *sgcb*$^{-/-}$ muscles (Figure 3A).

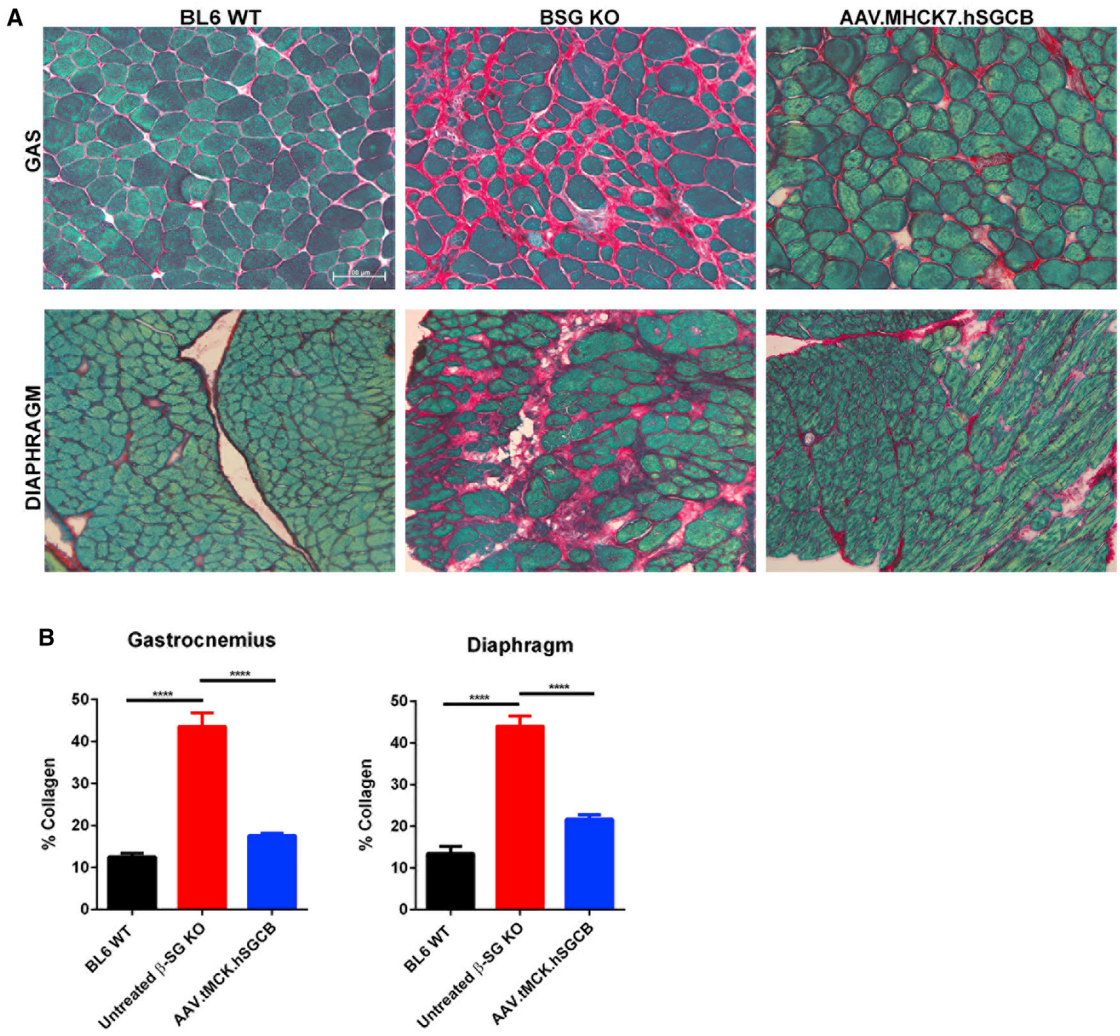

Figure 3. Reduced Collagen Deposition in Intravenously Treated β-SG KO Mice

(A) Picrosirius red staining shows reduced fibrosis in treated mice, indicated by a decrease in collagen deposition compared with untreated sgcb$^{-/-}$ mice in diaphragm and GAS. Representative 20× images are shown. Scale bar, 100 μm. (B) Quantification of collagen levels in the diaphragm and GAS muscles from C57BL/6 WT mice (n = 4), untreated *sgcb*$^{-/-}$ mice (n = 4), and treated *sgcb*$^{-/-}$ mice (n = 5) confirm reduction in collagen levels in both treated muscles ($p < 0.0001$).

Vector-transduced GAS muscle contained 17.55% ± 0.59% collagen compared with 43.55% ± 3.33% collagen in untreated *sgcb*$^{-/-}$ GAS muscles ($p < 0.0001$). Furthermore, treated diaphragm muscle exhibited 21.67% ± 1.09% collagen compared with 44.05% ± 2.39% in untreated *sgcb*$^{-/-}$ muscle ($p < 0.0001$) (Figure 3B), demonstrating the ability of hSGCB gene transfer to mitigate the fibrotic component of the LGMD2E phenotype.

Intravenous Gene Transfer to SGCB$^{-/-}$ Mice Reduces Kyphoscoliosis of the Thoracic Spine

We noted previously the involvement of the skeletal system in LGMD2E patients[8,11] as well as in mouse models of muscular dystrophy with the development of joint contractures and kyphoscoliosis (curvature) of the thoracic spine.[9,10] Degeneration of torso muscles because of the worsening histopathology discussed above can be attributed to kyphosis. As a result of the severity of the phenotype in the *sgcb*$^{-/-}$ mouse with the gross anatomical appearance of kyphoscoliosis, full-body X-ray radiography was used to determine the degree of kyphosis in 7-month-old BL6 WT mice, *sgcb*$^{-/-}$ mice, and treated *sgcb*$^{-/-}$ mice 6 months post-injection. The kyphotic index (KI) score determines a quantitative value for the level of kyphoscoliosis.[9] As depicted in Figure 4A, WT, the KI score is a ratio of length from forelimb to hindlimb compared with the length of the midline to the apex of the curvature in the spine. Although *sgcb*$^{-/-}$ mice present with a severely curved spine and lower a KI score of 3.64 ± 0.16, BL6 WT mice have a significantly straighter spine, resulting in a higher KI score of 6.01 ± 0.41 ($p < 0.01$) (Figure 4B). Treated *sgcb*$^{-/-}$ mice exhibit a significant reduction in the degree of kyphosis in the

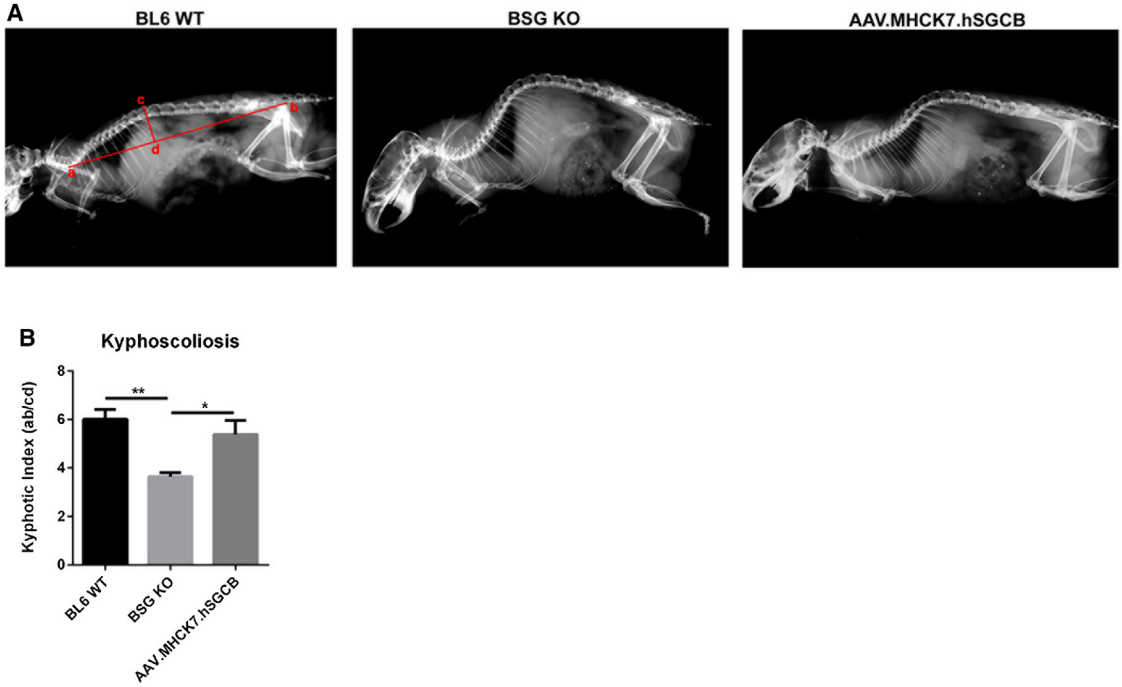

Figure 4. Correction of Kyphoscoliosis in Thoracic Spine

(A) Kyphoscoliosis in *sgcb*$^{-/-}$ mice as evident by X-ray radiography. (B) The KI score of *sgcb*$^{-/-}$mice (3.69) is low compared with C57BL/6 WT mice (6.01) ($p < 0.01$) but increases upon treatment with scAAVrh.74.MHCK7.hSGCB (5.39) ($p < 0.05$ compared with *sgcb*$^{-/-}$) (n = 6/group).

spine, with an increase in the KI score to 5.39 ± 0.58 ($p < 0.05$) (Figure 4B). These data indicated that intravenous delivery of scAAVrh.74.MHCK7.hSGCB is beneficial for the overall integrity of the spine and can alleviate the kyphosis and joint contractures present in the disease.

Assessment of Cardiomyopathy

The histological destruction of limb and diaphragm muscle presented above is also detected in the myocardium of 7-month-old *sgcb*$^{-/-}$ mice, particularly with the presence of myocardial necrosis and fibrosis, as evident by H&E and picrosirius red staining (Figure 5A). The presentation of impaired heart function in LGMD2E is often in the form of dilated cardiomyopathy with reduced cardiac output (CO) and a lower ejection fraction (EF).[8,13–16,19] We used cardiac MRI to evaluate several functional parameters of the heart to establish functional deficits in the myocardium of *sgcb*$^{-/-}$ mice compared with BL6 WT mice to use as a functional outcome measure. Imaging of control mice at 7 months of age showed a reduction of 29.3% in stroke volume (SV) from 0.041 ± 0.0019 mL in BL6 WT hearts to 0.029 ± 0.0024 mL in *sgcb*$^{-/-}$ hearts ($p < 0.01$), a 13.5% decrease in CO from 14.70 ± 0.74 mL/min in BL6 WT hearts to 12.72 ± 0.97 mL/min in *sgcb*$^{-/-}$ hearts ($p = 0.1349$), and finally a 14.0% lower EF, 66.21% ± 3.83% in *sgcb*$^{-/-}$ hearts compared with 76.90% ± 1.67% in BL6 WT hearts ($p < 0.05$) (Figure 5B). This indicates a modest decline in overall cardiac function at this age and a trend toward the development of cardiomyopathy. Restoring hSGCB expression in hearts of KO mice through systemic delivery partially corrected these deficits, improving SV to 0.032 ± 0.0027 mL, CO to 14.66 ± 0.75 mL/min, and the EF to 68.16% ± 2.31% (Figure 5B). As a correlate to the histological and functional disruption of cardiac tissue reported here, western blotting for cardiac troponin I (cTrpI) expression, an important indicator of cardiac damage, is reduced in diseased *sgcb*$^{-/-}$ hearts to 60.38% of the levels seen in BL6 WT mice (Figure 5C). The levels of cTrpI are restored following treatment to levels of 35.80% of the expression seen in WT hearts (Figure 5D).

Functional Restoration in the Diaphragm Muscle with an Increase in Physical Activity

We previously demonstrated that AAV-mediated hSGCB gene transfer can restore function to dystrophic *sgcb*$^{-/-}$ muscle.[18] Although the importance of these initial studies with an AAV.hSGCB vector containing the tMCK promoter focusing on limb skeletal muscle (specifically the functional properties of the TA) cannot be undermined, the significant involvement of diaphragm dysfunction and respiratory failure in LGMD2E mandate a functional benefit to the diaphragm essential for validation of clinical systemic therapy. With the use of an ex vivo experimental protocol on strips taken from diaphragm muscle, we assessed whether restoring β-sarcoglycan provides a functional benefit to this severely compromised muscle. In accordance with the significant histopathology identified in 7-month-old diaphragms from diseased mice, *sgcb*$^{-/-}$ diaphragms exhibited a functional deficit with a significant (51%) reduction in specific force

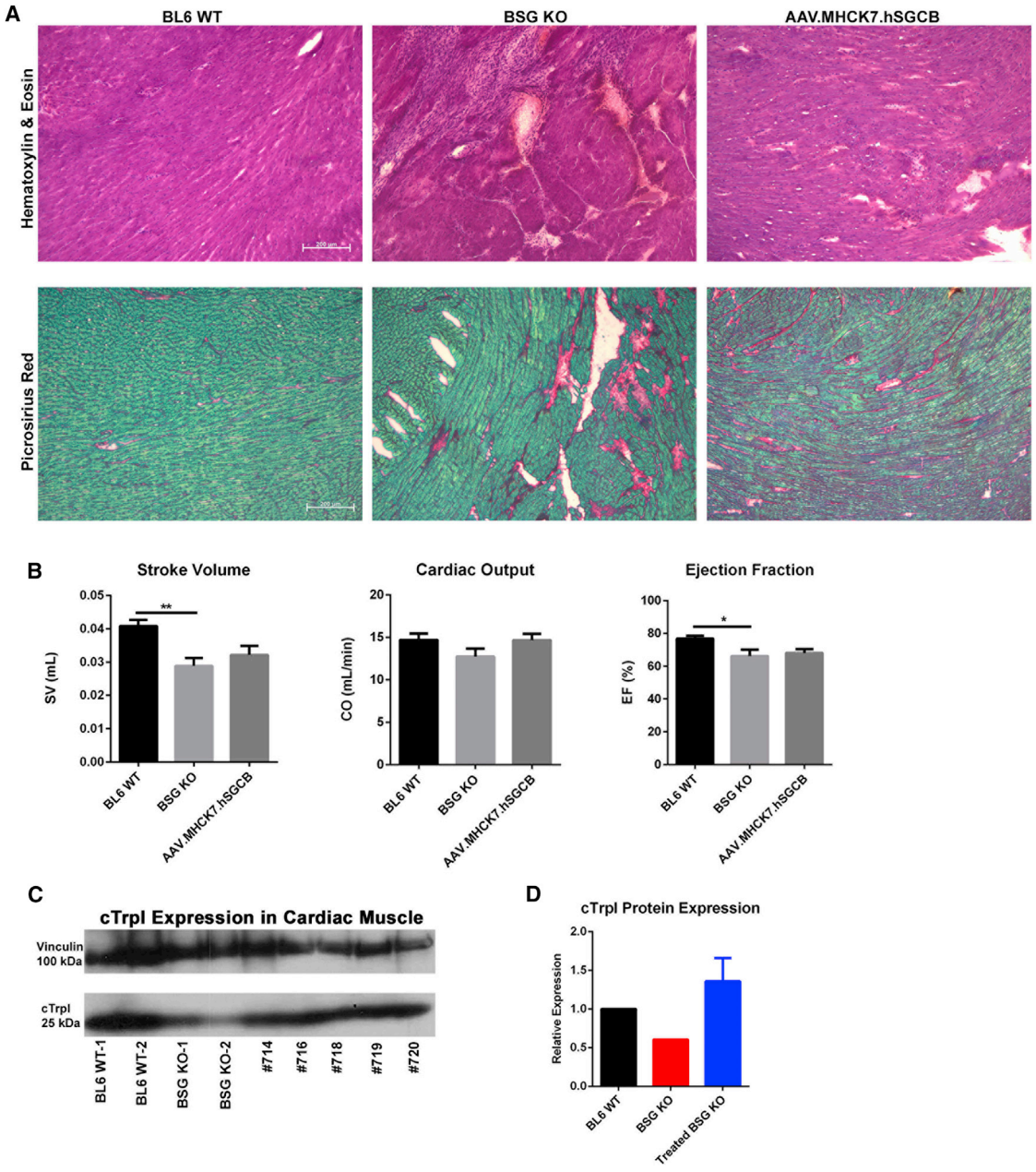

Figure 5. Assessment of Cardiomyopathy in Heart Muscle

(A) H&E and picrosirius red stains of 7-month-old BL6 WT, *sgcb*$^{-/-}$, and AAV.MHCK7.hSGCB-treated *sgcb*$^{-/-}$ hearts 6 months post-treatment, indicating myocardial degeneration in untreated *sgcb*$^{-/-}$ muscle and improvement following treatment. Representative 10× images are shown. Scale bar, 200 μm. (B) Cardiac MRI analysis showing reduction in *sgcb*$^{-/-}$ hearts in SV ($p < 0.01$), CO, and EF ($p < 0.05$) and improvements 6 months after treatment (n = 6/group). (C) Western blotting of two C57BL/6 WT hearts, two *sgcb*$^{-/-}$ hearts, and five AAV.MHCK7.hSGCB-treated *sgcb*$^{-/-}$ hearts showing decreased cardiac troponin I levels in diseased mice. (D) Densitometry quantification showing reduction of cTrpI to 60.38% of BL6 WT levels and an overexpression of up to 135.8% of BL6 WT levels.

output compared with BL6 WT mice (116.24 ± 10.49 mN/mm^2 versus 236.67 ± 15.87 mN/mm^2, respectively; $p < 0.001$) as well as a greater loss of force from that produced after the first contraction following a rigorous fatigue protocol (23% ± 1.0% loss in *sgcb*$^{-/-}$ and 7.0% ± 3.0% loss in BL6 WT, $p < 0.05$) (Figure 6A). Six months following tail vein delivery of scAAVrh.74.MHCK7.hSGCB, we noted a dramatic improvement in specific force output, which increased to 226.07 ± 27.12 mN/mm^2 ($p < 0.05$ compared with *sgcb*$^{-/-}$) and better protection of the muscle from repeated fatigue with only a 12.0% ± 4.0% loss of force ($p < 0.05$ compared with *sgcb*$^{-/-}$) (Figure 6A).

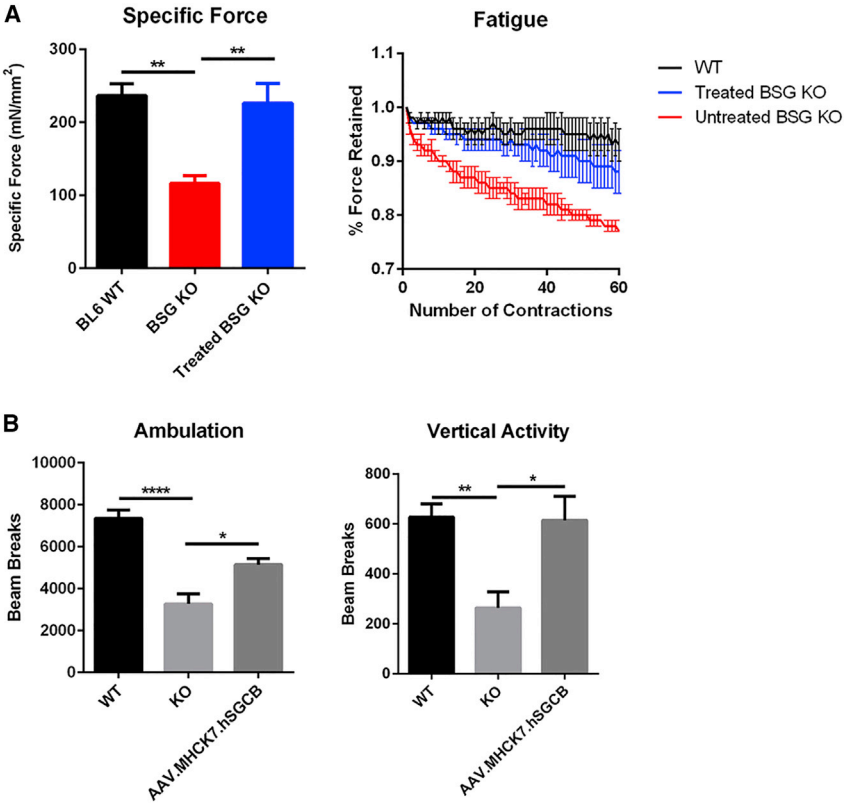

Figure 6. Diaphragm Function Correction and Increased Open-Field Cage Activity

(A) Diaphragm muscle strips were harvested to measure force and resistance to fatigue in BL6 WT mice (n = 5), *sgcb*$^{-/-}$ mice (n = 4), and AAV.MHCK7.hSGCB-treated *sgcb*$^{-/-}$ mice (n = 5), all at 7 months of age. Six months of treatment restored force to WT levels ($p < 0.01$ compared with *sgcb*$^{-/-}$) and improved resistance to fatigue. (B) Overall ambulation in the x and y planes is significantly decreased in *sgcb*$^{-/-}$ mice ($p < 0.0001$) and slightly improved in MCHK7-treated mice ($p < 0.05$). Vertical activity rearing onto the hindlimbs also decreased in *sgcb*$^{-/-}$ mice ($p < 0.01$) and significantly increased in MCHK7-treated mice ($p < 0.05$) (n = 6/group).

Overall, these data support our previous findings in the TA muscle and show that restoring β-sarcoglycan provides functional recovery in diaphragm muscle.

Symptoms of increased fatigue and reduced overall activity are frequently reported in many neuromuscular diseases.[27,28] partially attributed to the occurrence of kyphosis. As a result, and taking into account the phenotype of LGMD2E, we hypothesized that KO mice would naturally be less active compared with healthy WT mice and, moreover, that systemic delivery of rAAV.MHCK7.hSGCB to *sgcb*$^{-/-}$ mice would result in more physically active mice. To test this hypothesis and additional potential functional benefits of our gene transfer, laser monitoring of an open-field cage activity protocol similar to that used in previous reports[29,30] was performed on all groups of mice. The graphs in Figure 6B depict a significant decrease (55.5%) in knockout (KO) mice compared with the WT in both total ambulation (horizontal movement in the x and y planes) and hindlimb vertical rearing. The mean horizontal ambulatory laser beam breaks over a 1-hr period in WT mice was 7355.0 ± 400.8 compared with 3271.0 ± 483.8 in KO mice ($p < 0.0001$). Furthermore, the mean vertical rearing beam breaks recorded in WT mice was 627.0 ± 53.76 as opposed to 265.0 ± 63.36 in KO mice ($p < 0.01$) (Figure 6B). In accordance with our initial hypothesis, rAAV.MHCK7.hSGCB-treated mice were visibly more active compared with KO mice, which is illustrated in the quantification of activity, where total ambulation increased by 57% to 5143.0 ± 293.2 beam breaks ($p < 0.05$), and hindlimb vertical rearing increased dramatically by 132% to 615.0 ± 95.93 beam breaks ($p < 0.05$) in treated mice (Figure 6B).

Safety and Biodistribution Analysis of rAAVrh.74.MHCK7.hSGCB

We also assessed any potential toxicity or safety concerns of hSGCB gene therapy in *sgcb*$^{-/-}$ mice 6 months following systemic delivery of scAAVrh.74.MHCK7.hSGCB at a 1.0×10^{12} vg total dose (5×10^{13} vg/kg based on a 20-g mouse). Vector biodistribution and off-target transgene expression were analyzed on tissue samples (TA, TRI, diaphragm, heart, gonad, lungs, kidney, liver, and spleen) from vector-dosed *sgcb*$^{-/-}$ animals using qPCR and western blotting, respectively. Using vector-specific primer probe sets, MHCK7.hSGCB vg were detected at varying levels in all collected tissues. As expected, the highest levels were seen in the liver as well as in skeletal muscle and the heart, indicating that the test article was efficiently delivered into all intended muscles of vector-dosed mice (Figure 7A).

Furthermore, western blotting to detect hSGCB protein expression confirmed the functionality of the muscle-specific MHCK7 promoter and the expression of transgene restricted to cardiac and skeletal muscle. β-sarcoglycan protein expression was observed in varying amounts in all skeletal muscle samples as well as heart samples and, importantly, was not detected in any non-muscle tissue (Figure 7B), supported by the fact that β-sarcoglycan is known to be a muscle-specific protein. Finally, H&E staining was performed on muscle tissue and off-target organs harvested from these five *sgcb*$^{-/-}$ mice along with five C57BL6 WT mice treated systemically with our vector at the therapeutic dose used in this study (1×10^{12} vg total dose). These sections were then formally reviewed for toxicity by a veterinary pathologist. No adverse effects were detected in any sample from any of the mice, importantly noting the lack of toxicity in WT mice dosed with vector (Table S3). Taken together,

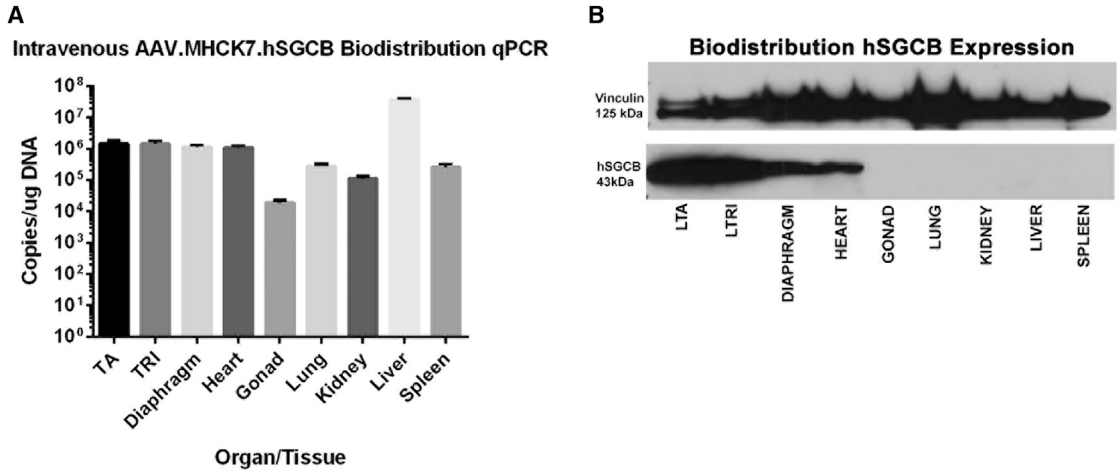

Figure 7. Biodistribution and Off-Target Transgene Expression Analysis of Systemic scAAVrh.74.MHCK7.hSGCB Delivery

(A) Distribution histogram of mean vg copies of transcript per microgram DNA added to qPCR reaction in various tissues from two *sgcb*$^{-/-}$ mice after intravenous (i.v.) delivery of scAAVrh.74.MHCK7.hSGCB at a 1e−12 vg total dose. (B) Biodistribution western blots on muscles and organs from scAAVrh.74.MHCK7.hSGCB systemically injected *sgcb*$^{-/-}$ mice, indicating no expression of the hSGCB transgene in any non-muscle samples.

these data indicate that this test article was well tolerated by the test animals.

DISCUSSION

This study investigated the use of intravenous gene transfer of recombinant adeno-associated virus (rAAV) carrying the human β-sarcoglycan (hSGCB) transgene as a promising new therapy for LGMD2E. Our investigations with AAV-mediated hSGCB gene therapy have utilized a self-complementary AAV to enhance transgene expression,[20,21] the rh.74 serotype for improved vascular delivery,[22,23,31] muscle-specific promoters to better target skeletal or cardiac muscle,[25,32,33] and the optimization of a human β-sarcoglycan gene (*hSGCB*) as advantages for clinical efficacy. In our previous studies demonstrating therapeutic efficacy using the tMCK promoter, the successful targeting of multiple muscles by vascular delivery to restore β-sarcoglycan expression along with the significant reduction of fibrosis, all leading to functional recovery, provided a foundation for translating AAV-mediated hSGCB transfer to LGMD2E patients.[18]

We know from initial reports characterizing the phenotype of the *sgcb*$^{-/-}$ mouse that it accurately recapitulates the clinical pathological features of LGMD2E,[4,5] providing an advantage for pre-clinical translational studies. Based on the histological and functional deficits in *sgcb*$^{-/-}$ diaphragms and hearts, targeting the diaphragm and cardiac muscles must be considered in the long-term treatment of this disease. Additionally, given the incidence of cardiomyopathy in patients representing a major limitation/long-term liability for treatment, exclusive targeting to achieve skeletal muscle correction may be insufficient and potentially harmful for the LGMD2E population. There are always concerns that if we do improve limb skeletal muscle strength by localized gene delivery without comparable cardiac improvement that we could potentially stress the heart even further.[34] Consequently, this signifies the necessity of systemic delivery and the importance of cardiac and diaphragm correction in creating an effective treatment for LGMD2E patients.

Following the modification of our therapeutic AAV vector with addition of the MHCK7 promoter, allowing for enhanced transgene expression in cardiac muscle,[25] we demonstrate that intravenous injection of scAAVrh.74.MHCK7.hSGCB leads to nearly complete transduction and restoration of hSGCB expression in limb skeletal muscles, diaphragm muscle, and, importantly, cardiac muscle (Figure 1). Of note, the most significant wave of degeneration/regeneration occurs at 3 weeks in *sgcb*$^{-/-}$ muscle,[5,17] indicated by centrally placed nuclei. Animals were treated following this insult, and, therefore, a complete reversal of centralized nuclei was not anticipated. With systemic gene transfer in mind, the substantial involvement of diaphragm dysfunction and respiratory failure implicated in multiple forms of muscular dystrophy, including LGMD2E,[8,12,35] and their corresponding mouse models[5,36–38] is one potentially life-threatening component of this disease. Because of deteriorating limb, diaphragm, and cardiac muscle function in many neuromuscular diseases, reports of increased fatigue and reduced overall activity are also seen.[27,28] We detail here the evidence of histological disruption of *sgcb*$^{-/-}$ diaphragm tissue at 7 months of age, which is accompanied by reduced diaphragm force outputs, parameters that are improved following gene transfer (Figures 2 and 6). Kyphoscoliosis of the thoracic spine because of weakening of muscles supporting the spinal column can result in the diaphragm being pushed forward, further compromising lung capacity and diaphragm function.[8–10] We were able to demonstrate the alleviation of kyphosis and increased physical activity in *sgcb*$^{-/-}$ mice following systemic delivery of our vector (Figures 4 and 6). Although no specific experiments to assess respiratory function were performed, the presence of kyphoscoliosis and the apparent

fatigue seen in the open-field activity cage provide evidence of impaired respiration, the parameters of which were improved following treatment, indicating the potential of therapy to improve the quality of life for LGMD2E patients.

The development of cardiomyopathy in LGMD2E occurs in up to 50% or more of patients, much more than with other LGMDs,[8,13–16] which suggests that compensatory mechanisms and other cardiac proteins can protect the heart in some forms of sarcoglycanopathy but not LGMD2E. For example, ε-sarcoglycan, an α-sarcoglycan homolog,[39] protects LGMD2D patients from heart involvement.[39,40] Mice deficient for SGCB show dystrophic myocardial pathology as early as 4 weeks of age,[4,5] findings we have reproduced; however, we found no correlation between the age of development of cardiac histopathology and the age of decline in cardiac function, with no significant cardiac deficits seen at 7 months of age (Figure 5). The age of mice analyzed along with the small sample size of each cohort contributed to the lack of significant deficits in cardiac functional parameters and lack of improved function seen here. We also hypothesize that treating mice at 4 weeks of age restores hSGCB expression after the initiation of the cardiac remodeling that occurs in the myocardium, therefore potentially limiting the ability to fully restore function. By treating mice earlier than 4 weeks of age (for example, newborn pups), it is feasible to fully restore the DAPC in the sarcolemma of cardiomyocytes prior to cardiac remodeling and fully protect them from degeneration. We also report in this study high levels of hSGCB expression in cardiomyocytes up to 72.0% greater than BL6 WT levels. We found no evidence of any detrimental effects on cardiac function because of this overexpression. hSGCB was correctly localized to the sarcolemma of cardiomyocytes along with SGCA and dystrophin, indicating restoration of the DAPC at the sarcolemma (Figure 1; Figure S1). Additionally, no evidence of toxicity was detected in healthy BL6 WT hearts treated intravenously with our vector and overexpressing hSGCB, as reported by an independent veterinary pathologist (Table S3). Eventually, hearts from aged (18 months) *sgcb*$^{-/-}$ mice do present with dilated cardiomyopathy symptoms with increased posterior wall thickening, increased ventricular diameters, and decreased fractional shortening.[19] We do see slight differences in SV, CO, and EF between BL6 WT hearts and β-sarcoglycan (BSG) KO hearts at the younger time point of 7 months; however, these small differences do not correspond to the manifestation of dilated cardiomyopathy at this age. We believe that these slight differences we report are seen because of the specific parameters that are used to calculate SV, CO, and EF parameters. Of these, we did see small differences between BL6 WT hearts and BSG KO hearts in end diastolic volumes (EDVs) and end systolic volumes (ESVs) as well as increased heart rate (HR) in BSG KO mice, all of which contribute to the reported changes in SV, CO, and EF between the two strains of mice. At a cellular level, these findings at 7 months are likely due to the degeneration of cardiomyocytes and fibrotic tissue deposition that begins at a very young age (~4–8 weeks); however, there is compensation for early cardiac remodeling, including the Frank-Starling mechanism and neurohormonal activation through the renin-angiotensin-aldosterone pathway.[41,42] Significant changes in EF and CO do not manifest until later in the disease process with the presence of overfibrotic scarring. Ultimately, the manifestation of cardiomyopathy symptoms in aged (18 months) *sgcb*$^{-/-}$ mice does provide a basis for our ongoing studies to show correction of these deficits following AAV treatment.

As a corollary to the functional assessment of cardiomyopathy, we performed western blotting for cTrpI on heart tissue from BL6 WT, untreated *sgcb*$^{-/-}$, and AAV.MHCK7.hSGCB-treated mice. cTrpI is an important regulator of cardiac function in cardiomyocytes and has been implicated as a biomarker for damage to the heart. A previous study showed a reduction in cTrpI levels in normal WT aging hearts that correlated with significant diastolic dysfunction observed by pressure-volume (P-V) loop and echocardiography analysis.[43] The authors also noted, using ultrastructural analysis, that WT aging hearts showed evidence of myocardial degeneration, sarcomere dissolution, and thickening of the Z line.[43] Therefore, the processes of cardiac remodeling that lead to reduced cardiac function in aging WT hearts are similar to the disease progression in *sgcb*$^{-/-}$ hearts, albeit less severe and with a later onset of myocardial damage compared with the disease state of *sgcb*$^{-/-}$ hearts. In agreement with lower cTrpI levels in the heart indicating impaired cardiac function, hearts from 7-month-old *sgcb*$^{-/-}$ mice show about 40% lower cTrpI levels compared with healthy BL6 WT hearts, levels that are restored to above WT levels in treated hearts. Importantly, when considering a clinically effective therapy for patients, the cardiac involvement in β-sarcoglycan deficiency does not correlate with age, muscle strength, or level of dystrophic changes on muscle biopsy.[8,13] We are currently exploring the use of cTrpI serum levels in our long-term studies to determine whether this can be effectively used as a biomarker for cardiomyopathy in LGMD2E.

Finally, *Sgcb*$^{-/-}$ mice and C57BL6 WT mice given an intravenous tail vein injection of scAAVrh.74.MHCK7.hSGCB at our proposed dose of 1×10^{12} vg total dose (5×10^{13} vg/kg) were fully necropsied for a pathology review by an independent veterinary pathologist. We know from previous studies that AAVrh.74 does transduce the liver; however, these studies, including our previous work with an AAVrh.74.hSGCB vector, showed no liver toxicity, aided by the use of a muscle-specific promoter.[18,22–24] As expected, in our current study, we detected high vg copy numbers in the livers of vector-dosed mice; however, we detected no hSGCB protein expression in the liver, indicating correct function of the muscle-specific MHCK7 promoter (Figure 7), and the findings from the independent veterinary pathologist review point to no evidence of toxicity in the liver from diseased *sgcb*$^{-/-}$ mice or healthy BL6 WT mice (Table S3). The fact that we achieve such high levels of transduction in all muscles throughout the body with no adverse effects using a lower dose relative to doses used in other gene therapy studies provides great promise for translation to LGMD2E patients. From a clinical perspective, the dose used here is lower than the dose used for systemic delivery of an *SMN1*-expressing AAV therapy delivered to babies with spinal muscular atrophy (SMA), which is currently in a clinical trial.[44,45] The highly efficient restoration of β-sarcoglycan expression using

the MHCK7 promoter accompanied by functional benefits is very encouraging at dosing levels that could be applied clinically, and given the high incidence of heart involvement in the β-sarcoglycan deficiency in LGMD2E patients, we feel that systemic delivery provides the greatest benefit to these patients and holds the greatest promise for treating this debilitating disease.

MATERIALS AND METHODS

Animal Models

All procedures were approved by The Research Institute at the Nationwide Children's Hospital Institutional Animal Care and Use Committee (protocol AR12-00040). B6.129-Sgcb $^{tm1Kcam/1J}$ heterozygous mice were purchased from The Jackson Laboratory (strain 006832). *Sgcb*$^{-/-}$ mice were generated by breeding heterozygous mice. KO mice were bred and maintained as homozygous animals under standardized conditions in the Animal Resources Core at the Research Institute at Nationwide Children's Hospital. Mice were maintained on Teklad Global Rodent Diet (3.8% fiber, 18.8% protein, 5% fat chow) with a 12:12-hr dark:light cycle. All animals were housed in standard mouse cages with food and water ad libitum.

Genotyping

DNA genotyping was used to identify *sgcb*$^{-/-}$ mice. DNA from tail clippings was isolated and analyzed by OneTaq DNA polymerase (New England Biolabs) PCR. A series of primers was used in the PCR analysis to determine the β-sarcoglycan knockout status. The set included a common primer complementary to a region outside of the mouse β-sarcoglycan gene in chromosome 5 (5′ CAG GAC AGT GCT CAG CAA GA 3′), a mutant primer complementary to the inserted neomycin knockout cassette (5′ GCC TGA AGA ACG AGA TCA GC 3′), a forward WT primer complementary to exon 4 (5′ TTT TTG ACC CAA GGA CAC A 3′), and a reverse WT primer complementary to exon 5 (5′ TTG CCC ATG ATG AAG ACG CC 3′). Reactions were carried out on genomic DNA for 30 cycles under the following conditions: 94°C, 30 s; 57°C, 30 s; 68°C, 20 s.

β-Sarcoglycan Gene Construction

The full-length human β-sarcoglycan cDNA (GenBank: NM_0034994.3) was codon-optimized and synthesized by GenScript. The cDNA was then cloned into a scAAVrh.74 vector (for enhanced transduction via vascular delivery) containing AAV2 inverted terminal repeats (ITRs), and the cassette includes a consensus Kozak sequence (CCACC), an SV40 chimeric intron, and a synthetic polyadenylation site (53 bp). The recombinant MHCK7 promoter used to drive transgene expression is a muscle-specific promoter and was a gift from Dr. Steven Hauschka (University of Washington). This is an MCK-based promoter that utilizes a 206-bp enhancer taken from ~1.2 kb 5′ of the transcription start site within the endogenous muscle CK gene with a proximal promoter (enh358MCK, 584 bp).[25] This enhancer, along with a modified CK7 cassette from the MCK family of genes, is ligated to a 188-bp α-myosin heavy chain (α-MyHC) enhancer 5′ of the CK portion to enhance cardiac expression.[25] The CK portion of the promoter is 96% identical between tMCK and MHCK7. Finally, the pAAV.MHCK7.hSGCB vector was constructed by ligation of the 960-bp NotI/KpnI MHCK7+Intron fragment from pAAV.MHCK7.-DYSF5′DV[46] into the NotI/KpnI sites of pAAV.tMCK.hSGCB.[18]

rAAV Production

A revised AAV cross-packaging approach reported previously[31] was used to produce the recombinant AAV vector. Here, a triple transfection method with $CaPO_4$ precipitation in HEK293 cells allows for AAV2 ITRs to be packaged into a different AAV capsid serotype.[47,48] The production plasmids were pAAV.MHCK7.hSGCB, rep2-caprh.74 modified AAV helper plasmids encoding cap serotype 8-like isolate rh.74, and an adenovirus type 5 helper plasmid (pAd-helper) expressing adenovirus E2A, E4 ORF6, and VA I/II RNA genes. Vectors were purified, and the encapsulated vg titer (utilizing a Prism 7500 Taqman detector system, PE Applied Biosystems) was determined as described previously.[49] The primer and fluorescent probe targeted the MHCK7 promoter and were as follows: MHCK7 forward primer, 5′-CCA ACA CCT GCT GCC TCT AAA-3′; MHCK7 reverse primer, 5′-GTC CCC CAC AGC CTT GTT C-3′; MHCK7 probe, 5′-FAM-TGG ATC CCC-Zen-TGC ATG CGA AGA TC-3IABKFQ-3′.

Gene Delivery

Systemic delivery was achieved through injection of vector into the tail vein of *sgcb*$^{-/-}$ mice. Mice were injected with a 1×10^{12} vg total dose (mice ranging from 13–20 g, 5×10^{13} vg/kg based on a 20-g mouse) of scAAVrh.74.MHCK7.hSGCB diluted in saline in a 212-μL volume using a 30G ultra-fine insulin syringe. Mice were restrained in a holding tube, placing the tail back through a tail slot to warm it up to dilate the blood vessels for ease of injection. After locating the artery down the center line of the tail, the injection was performed in one of the purple/blue lateral veins that run alongside the tail artery. All treated mice were injected at 4-5 weeks of age and euthanized 6 months post-injection.

Serum CK Measurement

Levels of CK were measured in the sera of BL6 WT mice (n = 6), untreated *sgcb*$^{-/-}$ mice (n = 4), and rAAV.MHCK7.hSGCB-treated *sgcb*$^{-/-}$ mice (n = 6) using the CK-SL assay kit and the corresponding manufacturer's protocol from Sekisui Diagnostics (catalog no. 326-10). Briefly, 25 μL of serum was mixed with 1 mL of the working reagents and added to a cuvette. A kinetic assay was set on the spectrophotometer to measure the absorbance at 340 nm every 30 s for 180 s. CK levels were calculated using the absorbance readings and the equation listed below.

$$\begin{aligned} \mathrm{U/L} &= [(\Delta \mathrm{Abs./min}) \times 1.025 \times 1,000]/[1 \times 6.22 \times 0.025] \\ &= (\Delta \mathrm{Abs./min}) \times 6,592 \end{aligned}$$

Diaphragm Tetanic Contraction for Functional Assessment

Mice were euthanized, and the diaphragm was dissected with rib attachments and central tendon intact and placed in Kreb's-Henseleit (K-H) buffer as described previously.[30,50,51] A 2- to 4-mm-wide section of diaphragm was isolated. Diaphragm strips were tied firmly

with braided surgical silk (6/0, Surgical Specialties) at the central tendon and sutured through a portion of rib bone affixed to the distal end of the strip. Each muscle was transferred to a water bath filled with oxygenated K-H solution that was maintained at 37°C. The muscles were aligned horizontally and tied directly between a fixed pin and a dual-mode force transducer servomotor (305C, Aurora Scientific). Two platinum plate electrodes were positioned in the organ bath to flank the length of the muscle. The muscle was stretched to optimal length for measurement of twitch contractions and then allowed to rest for 10 min before initiation of the tetanic protocol. When the muscle was stabilized, the muscle was set to an optimal tension of 1 g and subjected to a warm-up that consisted of three 1-Hz twitches every 30 s followed by three 150-Hz twitches every minute. After a 3-min rest period, the diaphragm was stimulated at 20, 50, 80, 120, 150, and 180 Hz, allowing a 2-min rest period between each stimulus, each with a duration of 250 ms to determine maximum tetanic force. Muscle length and weight were measured. The force was normalized for muscle weight and length.

Cardiac MRI

Cardiac function was analyzed using a 9.4T horizontal bore MRI system and mouse volume coil (Bruker BioSpin). Mice were anaesthetized with 2.5% isoflurane mixed with carbogen (1 L/min) for 3 min prior to placement on the imaging bed. Upon placement of mice in the imaging apparatus and initiation of imaging, the isoflurane/carbogen mixture was dropped to 1.5% for the remainder of the study. Electrocardiogram (EKG) and respiration were monitored using an MRI-compatible system (model 1025, Small Animal Instruments). Gated cardiac short-axis fast low angle short (FLASH) cine T1-weighted images were acquired over the entire left ventricle (LV) of the mouse (repetition time [TR] = 8 ms; echo time [TE] = 2.8 ms; α = 18°; matrix = 256 × 256; field of view (FOV) = 3.0 × 3.0 cm; slice thickness = 1 mm, nslices = 7, up to 20 frames per cardiac cycle). For image analysis, the end-diastolic and end-systolic time point of each short-axis image were identified, and the endocardial and epicardial cardiac boundaries were manually traced. The papillary muscles were excluded from the endocardial boundary of the LV. From these measured areas, EDV, ESV, SV, CO, EF, and mean LV mass were calculated. Individual comparisons between BL6 WT hearts and sgcb$^{-/-}$ hearts for SV, CO, and EF were made using an unpaired two-tailed t test, and p values for comparisons that were not statistically significant are included in Results.

Immunofluorescence

Cryosections (12 μm) from the TA, GAS, QUAD, PSOAS), GLUT, TRI, and diaphragm muscles along with the heart were subjected to immunofluorescence staining for the hSGCB transgene via our previously used protocol.[18] Sections were incubated with a mouse monoclonal human β-sarcoglycan primary antibody (Leica Biosystems, catalog no. NCL-L-b-SARC) at a dilution of 1:100. Four random 20× images covering the four different quadrants of the muscle section were taken using a Zeiss AxioCam MRC5 camera. The percentage of fibers positive for β-sarcoglycan staining (>50% of muscle membrane staining) was determined for each image and averaged for each muscle.

Western Blot Analysis

Western blots were performed according to our previously used protocol, with several modifications specific for each antibody used.[18] Samples from C57BL6 WT mice, untreated *sgcb*$^{-/-}$ mice, and vector-dosed *sgcb*$^{-/-}$ mice were used for each western blot. A 1:250 dilution of a rabbit polyclonal human β-sarcoglycan antibody (Novus Biologicals, catalog no. NBP-1-90300) and a 1:5,000 dilution of a mouse monoclonal α-actinin antibody (Sigma-Aldrich, catalog no. A7811) were used for hSGCB blots. A 1:500 dilution of a rabbit polyclonal mouse cardiac troponin I antibody (Abcam, catalog no. ab47003) and a 1:1,000 dilution of a rabbit monoclonal mouse vinculin antibody (Invitrogen, catalog no. 70062) were also used. Anti-mouse (Millipore, catalog no. AP308P) and anti-rabbit (Life Technologies, catalog no. 656120) secondary horseradish peroxidase (HRP) antibodies were used for enhanced chemiluminescence (ECL) immunodetection. Western blot quantification was performed through densitometry using ImageQuantTL 1D 8.1.0 (GE Healthcare Life Sciences).

Morphometric Analysis

H&E staining was performed on 12-μm-thick cryosections of muscle from 7-month-old C57BL6 WT mice (n = 5), *sgcb*$^{-/-}$ mice (n = 5), and rAAV.MHCK7.hSGCB 6-month-treated *sgcb*$^{-/-}$ mice (n = 5) for analysis. The percentage of myofibers with central nuclei was determined in the TA, GAS, QUAD, PSOAS, GLUT, TRI, and diaphragm muscles. Additionally, muscle fiber diameters were measured in the GAS, PSOAS, and TRI muscles. Four random 20× images per muscle per animal were taken with a Zeiss AxioCam MRC5 camera. Centrally nucleated fibers were quantified using the NIH ImageJ software, and fiber diameters were measured using Zeiss Axiovision LE4 software.

Biodistribution qPCR Analysis

Taqman qPCR was performed to quantify the number of vg copies present in targeted and untargeted contralateral muscle as well as non-targeted organs as described previously.[18,23,49] A vector-specific primer probe set was used to amplify a sequence of the intronic region directly downstream of the MHCK7 promoter that is unique and located within the scAAVrh.74.MHCK7.hSGCB transgene cassette. The following primers and probe were used in this study: MHCK7 intron forward primer 5′-GTG AGG CAC TGG GCA GGT AA-3′, MHCK7 intron reverse primer 5′-ACC TGT GGA GAG AAA GGC AAA G-3′, and MHCK7 intron probe 5′-6FAM-ATC AAG GTT ACA AGA CAG-GTT TAA GGA GAC CAA TAG AAA-TAMRA-3′ (Integrated DNA Technologies). The copy number is reported as vg per microgram of genomic DNA.

Picrosirius Red Stain and Collagen Quantification

A protocol to determine the levels of collagen deposition in muscle tissue was performed on 12-μm cryosections from 7-month-old C57BL6 WT (n = 4), untreated *sgcb*$^{-/-}$ (n = 4), and rAAV.MHCK7.hSGCB 6-month-treated *sgcb*$^{-/-}$ (n = 5) GAS and

diaphragm muscles. A slightly amended protocol we published previously was used in this study.[18] Solution A (phosphomolydbic acid) was not used in this experimental protocol. Sections were placed straight in solution B (Direct Red 80/2 4 6-trinitrophenol) for 15 min following incubation in 10% neutral buffered formalin and a distilled water rinse. Here again four 20× images were taken per muscle per mouse, and the mean percent collagen for each muscle was then calculated for all groups.

X-Ray Images

Whole-body X-rays were performed on anesthetized 7-month-old C57BL6 WT mice (n = 6), untreated *sgcb*$^{-/-}$ mice (n = 6), and rAAV.MHCK7.hSGCB 6-month-treated *sgcb*$^{-/-}$ mice (n = 6) using the Faxitron MX-20 digital X-ray system at 26 kV for 3 s (Faxitron X-Ray).

Laser Monitoring of Open-Field Cage Activity

An open-field activity chamber was used to determine the overall activity of the experimental mice. Mice at 7 months of age from the C57BL6 WT (n = 6) and untreated *sgcb*$^{-/-}$ (n = 6) control groups along with rAAV.MHCK7.hSGCB 6-month-treated *sgcb*$^{-/-}$ mice (n = 6) were subjected to analysis following a previously described protocol[29,30] with several modifications. All mice were tested at the same time of day in the early morning near the end of the night cycle, when mice are most active. All mice were tested in an isolated room under dim light and with the same handler each time. Also, as was done in the previous reports, to reduce anxiety and keep behavioral variables at a minimum that could potentially affect normal activity of the mice and consequently the results of the assay, we tested mice that were not individually housed.[52] Mice were activity-monitored using the Photobeam activity system (San Diego Instruments). This system uses a grid of invisible infrared light beams that traverse the animal chamber front to back and left to right to monitor the position and movement of the mouse within an x-y-z plane. Activity was recorded for 1-hr cycles at 5-min intervals. Mice were acclimatized to the activity test room for an initial 1-hr session several days prior to beginning data acquisition. Mice were tested in individual chambers in sets of four. The testing equipment was cleaned between each use to reduce mouse reactionary behavioral variables that could alter our results. The data collected were converted to a Microsoft Excel worksheet, and all calculations were done within the Excel program. Individual beam breaks for movement in the x and y planes were added up for each mouse to represent total ambulation, and beam breaks in the z plane were added up to obtain vertical activity within the 1-hr time interval.

Statistical Analysis

Data were expressed as the mean ± SEM (error bars) and analyzed using one-way ANOVA with multiple comparisons between groups, and statistical significance determined through Tukey's post hoc analysis test using GraphPad Prism 5 (GraphPad) unless otherwise specified. Asterisks in the figures and reported data denote the level of statistical significance as follows: ns, no significance; *$p < 0.05$; **$p < 0.01$; ***$p < 0.001$; ****$p < 0.0001$.

SUPPLEMENTAL INFORMATION

Supplemental Information includes two figures and three tables and can be found with this article online at http://dx.doi.org/10.1016/j.ymthe.2017.02.013.

AUTHOR CONTRIBUTIONS

E.R.P., J.R.M., and L.R.R.K. conceived and designed the experiments. E.R.P. cloned the MHCK7 promoter into the original pAAV.tMCK.hSGCB plasmid and prepared the pAAV.MHCK7.hSGCB plasmid. E.R.P. and D.A.G. performed all tissue sectioning, immunofluorescence, and histology experiments. E.R.P. performed all morphometric data analyses. E.R.P. performed all western blotting and qPCR experiments. K.N.H. performed all diaphragm physiology experiments and data analyses. E.R.P. performed all X-ray radiography/kyphosis experiments and open-field cage activity experiments and data analyses. E.R.P. and L.R.R.K. wrote the manuscript. All authors reviewed, edited, and approved the manuscript.

CONFLICTS OF INTEREST

The authors have no conflicts of interest to disclose.

ACKNOWLEDGMENTS

We thank the Nationwide Children's Viral Vector Core for vector production. We would also like to thank Terri Shaffer, MLAS, RLATG, for performing intravenous tail vein injections. We also want to thank the Small Animal Imaging Core at The Ohio State University Wexner Medical Center for performing all MRI analyses. Finally, we would like to thank Dr. Stephen Hauschka for his gift of the MHCK7 promoter. This work has been supported by Families belonging to the GFB Italian Onlus (a non-profit organization), the Center for Clinical and Translational Science voucher program at The Ohio State University Wexner Medical Center (UL1TR001070), and the Nationwide Children's Hospital Foundation (to L.R.R.K.).

REFERENCES

1. Moore, S.A., Shilling, C.J., Westra, S., Wall, C., Wicklund, M.P., Stolle, C., Brown, C.A., Michele, D.E., Piccolo, F., Winder, T.L., et al. (2006). Limb-girdle muscular dystrophy in the United States. J. Neuropathol. Exp. Neurol. *65*, 995–1003.

2. Bönnemann, C.G., Modi, R., Noguchi, S., Mizuno, Y., Yoshida, M., Gussoni, E., McNally, E.M., Duggan, D.J., Angelini, C., and Hoffman, E.P. (1995). Beta-sarcoglycan (A3b) mutations cause autosomal recessive muscular dystrophy with loss of the sarcoglycan complex. Nat. Genet. *11*, 266–273.

3. Bönnemann, C.G., Passos-Bueno, M.R., McNally, E.M., Vainzof, M., de Sá Moreira, E., Marie, S.K., Pavanello, R.C., Noguchi, S., Ozawa, E., Zatz, M., and Kunkel, L.M. (1996). Genomic screening for beta-sarcoglycan gene mutations: missense mutations may cause severe limb-girdle muscular dystrophy type 2E (LGMD 2E). Hum. Mol. Genet. *5*, 1953–1961.

4. Araishi, K., Sasaoka, T., Imamura, M., Noguchi, S., Hama, H., Wakabayashi, E., Yoshida, M., Hori, T., and Ozawa, E. (1999). Loss of the sarcoglycan complex and sarcospan leads to muscular dystrophy in beta-sarcoglycan-deficient mice. Hum. Mol. Genet. *8*, 1589–1598.

5. Durbeej, M., Cohn, R.D., Hrstka, R.F., Moore, S.A., Allamand, V., Davidson, B.L., Williamson, R.A., and Campbell, K.P. (2000). Disruption of the beta-sarcoglycan gene reveals pathogenetic complexity of limb-girdle muscular dystrophy type 2E. Mol. Cell *5*, 141–151.

6. Angelini, C., Fanin, M., Freda, M.P., Duggan, D.J., Siciliano, G., and Hoffman, E.P. (1999). The clinical spectrum of sarcoglycanopathies. Neurology *52*, 176–179.

7. Sandonà, D., and Betto, R. (2009). Sarcoglycanopathies: molecular pathogenesis and therapeutic prospects. Expert Rev. Mol. Med. *11*, e28.

8. Semplicini, C., Vissing, J., Dahlqvist, J.R., Stojkovic, T., Bello, L., Witting, N., Duno, M., Leturcq, F., Bertolin, C., D'Ambrosio, P., et al. (2015). Clinical and genetic spectrum in limb-girdle muscular dystrophy type 2E. Neurology *84*, 1772–1781.

9. Laws, N., and Hoey, A. (2004). Progression of kyphosis in mdx mice. J. Appl. Physiol. *97*, 1970–1977.

10. Deconinck, A.E., Rafael, J.A., Skinner, J.A., Brown, S.C., Potter, A.C., Metzinger, L., Watt, D.J., Dickson, J.G., Tinsley, J.M., and Davies, K.E. (1997). Utrophin-dystrophin-deficient mice as a model for Duchenne muscular dystrophy. Cell *90*, 717–727.

11. Kaindl, A.M., Jakubiczka, S., Lücke, T., Bartsch, O., Weis, J., Stoltenburg-Didinger, G., Aksu, F., Oexle, K., Koehler, K., and Huebner, A. (2005). Homozygous microdeletion of chromosome 4q11-q12 causes severe limb-girdle muscular dystrophy type 2E with joint hyperlaxity and contractures. Hum. Mutat. *26*, 279–280.

12. Politano, L., Nigro, V., Passamano, L., Petretta, V., Comi, L.I., Papparella, S., Nigro, G., Rambaldi, P.F., Raia, P., Pini, A., et al. (2001). Evaluation of cardiac and respiratory involvement in sarcoglycanopathies. Neuromuscul. Disord. *11*, 178–185.

13. Fanin, M., Melacini, P., Boito, C., Pegoraro, E., and Angelini, C. (2003). LGMD2E patients risk developing dilated cardiomyopathy. Neuromuscul. Disord. *13*, 303–309.

14. Sveen, M.L., Thune, J.J., Køber, L., and Vissing, J. (2008). Cardiac involvement in patients with limb-girdle muscular dystrophy type 2 and Becker muscular dystrophy. Arch. Neurol. *65*, 1196–1201.

15. Melacini, P., Fanin, M., Duggan, D.J., Freda, M.P., Berardinelli, A., Danieli, G.A., Barchitta, A., Hoffman, E.P., Dalla Volta, S., and Angelini, C. (1999). Heart involvement in muscular dystrophies due to sarcoglycan gene mutations. Muscle Nerve *22*, 473–479.

16. Barresi, R., Di Blasi, C., Negri, T., Brugnoni, R., Vitali, A., Felisari, G., Salandi, A., Daniel, S., Cornelio, F., Morandi, L., and Mora, M. (2000). Disruption of heart sarcoglycan complex and severe cardiomyopathy caused by beta sarcoglycan mutations. J. Med. Genet. *37*, 102–107.

17. Gibertini, S., Zanotti, S., Savadori, P., Curcio, M., Saredi, S., Salerno, F., Andreetta, F., Bernasconi, P., Mantegazza, R., and Mora, M. (2014). Fibrosis and inflammation are greater in muscles of beta-sarcoglycan-null mouse than mdx mouse. Cell Tissue Res. *356*, 427–443.

18. Pozsgai, E.R., Griffin, D.A., Heller, K.N., Mendell, J.R., and Rodino-Klapac, L.R. (2016). β-Sarcoglycan gene transfer decreases fibrosis and restores force in LGMD2E mice. Gene Ther. *23*, 57–66.

19. Quattrocelli, M., Crippa, S., Montecchiani, C., Camps, J., Cornaglia, A.I., Boldrin, L., Morgan, J., Calligaro, A., Casasco, A., Orlacchio, A., et al. (2013). Long-term miR-669a therapy alleviates chronic dilated cardiomyopathy in dystrophic mice. J. Am. Heart Assoc. *2*, e000284.

20. McCarty, D.M., Fu, H., Monahan, P.E., Toulson, C.E., Naik, P., and Samulski, R.J. (2003). Adeno-associated virus terminal repeat (TR) mutant generates self-complementary vectors to overcome the rate-limiting step to transduction in vivo. Gene Ther. *10*, 2112–2118.

21. McCarty, D.M., Monahan, P.E., and Samulski, R.J. (2001). Self-complementary recombinant adeno-associated virus (scAAV) vectors promote efficient transduction independently of DNA synthesis. Gene Ther. *8*, 1248–1254.

22. Chicoine, L.G., Rodino-Klapac, L.R., Shao, G., Xu, R., Bremer, W.G., Camboni, M., Golden, B., Montgomery, C.L., Shontz, K., Heller, K.N., et al. (2014). Vascular delivery of rAAVrh74.MCK.GALGT2 to the gastrocnemius muscle of the rhesus macaque stimulates the expression of dystrophin and laminin alpha2 surrogates. Mol. Ther. *22*, 713–724.

23. Rodino-Klapac, L.R., Montgomery, C.L., Bremer, W.G., Shontz, K.M., Malik, V., Davis, N., Sprinkle, S., Campbell, K.J., Sahenk, Z., Clark, K.R., et al. (2010). Persistent expression of FLAG-tagged micro dystrophin in nonhuman primates following intramuscular and vascular delivery. Mol. Ther. *18*, 109–117.

24. Chicoine, L.G., Montgomery, C.L., Bremer, W.G., Shontz, K.M., Griffin, D.A., Heller, K.N., Lewis, S., Malik, V., Grose, W.E., Shilling, C.J., et al. (2014). Plasmapheresis eliminates the negative impact of AAV antibodies on microdystrophin gene expression following vascular delivery. Mol. Ther. *22*, 338–347.

25. Salva, M.Z., Himeda, C.L., Tai, P.W., Nishiuchi, E., Gregorevic, P., Allen, J.M., Finn, E.E., Nguyen, Q.G., Blankinship, M.J., Meuse, L., et al. (2007). Design of tissue-specific regulatory cassettes for high-level rAAV-mediated expression in skeletal and cardiac muscle. Mol. Ther. *15*, 320–329.

26. Narayanaswami, P., Weiss, M., Selcen, D., David, W., Raynor, E., Carter, G., Wicklund, M., Barohn, R.J., Ensrud, E., Griggs, R.C., et al.; Guideline Development Subcommittee of the American Academy of Neurology; Practice Issues Review Panel of the American Association of Neuromuscular & Electrodiagnostic Medicine (2014). Evidence-based guideline summary: diagnosis and treatment of limb-girdle and distal dystrophies: report of the guideline development subcommittee of the American Academy of Neurology and the practice issues review panel of the American Association of Neuromuscular & Electrodiagnostic Medicine. Neurology *83*, 1453–1463.

27. Schillings, M.L., Kalkman, J.S., Janssen, H.M., van Engelen, B.G., Bleijenberg, G., and Zwarts, M.J. (2007). Experienced and physiological fatigue in neuromuscular disorders. Clin. Neurophysiol. *118*, 292–300.

28. Kalkman, J.S., Schillings, M.L., Zwarts, M.J., van Engelen, B.G., and Bleijenberg, G. (2007). The development of a model of fatigue in neuromuscular disorders: a longitudinal study. J. Psychosom. Res. *62*, 571–579.

29. Kobayashi, Y.M., Rader, E.P., Crawford, R.W., Iyengar, N.K., Thedens, D.R., Faulkner, J.A., Parikh, S.V., Weiss, R.M., Chamberlain, J.S., Moore, S.A., and Campbell, K.P. (2008). Sarcolemma-localized nNOS is required to maintain activity after mild exercise. Nature *456*, 511–515.

30. Beastrom, N., Lu, H., Macke, A., Canan, B.D., Johnson, E.K., Penton, C.M., Kaspar, B.K., Rodino-Klapac, L.R., Zhou, L., Janssen, P.M., and Montanaro, F. (2011). mdx(^{5}cv) mice manifest more severe muscle dysfunction and diaphragm force deficits than do mdx Mice. Am. J. Pathol. *179*, 2464–2474.

31. Rodino-Klapac, L.R., Janssen, P.M., Montgomery, C.L., Coley, B.D., Chicoine, L.G., Clark, K.R., and Mendell, J.R. (2007). A translational approach for limb vascular delivery of the micro-dystrophin gene without high volume or high pressure for treatment of Duchenne muscular dystrophy. J. Transl. Med. *5*, 45.

32. Wang, B., Li, J., Fu, F.H., Chen, C., Zhu, X., Zhou, L., Jiang, X., and Xiao, X. (2008). Construction and analysis of compact muscle-specific promoters for AAV vectors. Gene Ther. *15*, 1489–1499.

33. Rodino-Klapac, L.R., Lee, J.S., Mulligan, R.C., Clark, K.R., and Mendell, J.R. (2008). Lack of toxicity of alpha-sarcoglycan overexpression supports clinical gene transfer trial in LGMD2D. Neurology *71*, 240–247.

34. Wasala, N.B., Bostick, B., Yue, Y., and Duan, D. (2013). Exclusive skeletal muscle correction does not modulate dystrophic heart disease in the aged mdx model of Duchenne cardiomyopathy. Hum. Mol. Genet. *22*, 2634–2641.

35. Khirani, S., Ramirez, A., Aubertin, G., Boulé, M., Chemouny, C., Forin, V., and Fauroux, B. (2014). Respiratory muscle decline in Duchenne muscular dystrophy. Pediatr. Pulmonol. *49*, 473–481.

36. Anderson, J.E., Garrett, K., Moor, A., McIntosh, L., and Penner, K. (1998). Dystrophy and myogenesis in mdx diaphragm muscle. Muscle Nerve *21*, 1153–1165.

37. Ishizaki, M., Suga, T., Kimura, E., Shiota, T., Kawano, R., Uchida, Y., Uchino, K., Yamashita, S., Maeda, Y., and Uchino, M. (2008). Mdx respiratory impairment following fibrosis of the diaphragm. Neuromuscul. Disord. *18*, 342–348.

38. Burns, D.P., Edge, D., O'Malley, D., and O'Halloran, K.D. (2015). Respiratory Control in the mdx Mouse Model of Duchenne Muscular Dystrophy. Adv. Exp. Med. Biol. *860*, 239–244.

39. Imamura, M., Mochizuki, Y., Engvall, E., and Takeda, S. (2005). Epsilon-sarcoglycan compensates for lack of alpha-sarcoglycan in a mouse model of limb-girdle muscular dystrophy. Hum. Mol. Genet. *14*, 775–783.

40. Cohn, R.D., Durbeej, M., Moore, S.A., Coral-Vazquez, R., Prouty, S., and Campbell, K.P. (2001). Prevention of cardiomyopathy in mouse models lacking the smooth muscle sarcoglycan-sarcospan complex. J. Clin. Invest. *107*, R1–R7.

41. Weil, J., Eschenhagen, T., Hirt, S., Magnussen, O., Mittmann, C., Remmers, U., and Scholz, H. (1998). Preserved Frank-Starling mechanism in human end stage heart failure. Cardiovasc. Res. *37*, 541–548.

42. Sigurdsson, A., and Swedberg, K. (1996). The role of neurohormonal activation in chronic heart failure and postmyocardial infarction. Am. Heart J. *132* (1 Pt 2 Su), 229–234.

43. Pan, B., Xu, Z.W., Xu, Y., Liu, L.J., Zhu, J., Wang, X., Nan, C., Zhang, Z., Shen, W., Huang, X.P., and Tian, J. (2016). Diastolic dysfunction and cardiac troponin I decrease in aging hearts. Arch. Biochem. Biophys. *603*, 20–28.

44. Mendell, J.R., Al-Zaidy, S., Shell, R., Arnold, W.D., Rodino-Klapac, L., Kissel, J.T., Prior, T.W., Miranda, C., Lowes, L., Alfano, L., et al. (2016). Gene Therapy for Spinal Muscular Atrophy Type 1 Shows Potential to Improve Survival and Motor Functional Outcomes. Mol. Ther. *24*, S190.

45. Mendell, J.R. (2014). Phase I Gene Transfer Clinical Trial for Spinal Muscular Atrophy Type 1 Delivering AVXS-101. http://adisinsight.springer.com/trials/700246826.

46. Sondergaard, P.C., Griffin, D.A., Pozsgai, E.R., Johnson, R.W., Grose, W.E., Heller, K.N., Shontz, K.M., Montgomery, C.L., Liu, J., Clark, K.R., et al. (2015). AAV.Dysferlin Overlap Vectors Restore Function in Dysferlinopathy Animal Models. Ann. Clin. Transl. Neurol. *2*, 256–270.

47. Rabinowitz, J.E., Rolling, F., Li, C., Conrath, H., Xiao, W., Xiao, X., and Samulski, R.J. (2002). Cross-packaging of a single adeno-associated virus (AAV) type 2 vector genome into multiple AAV serotypes enables transduction with broad specificity. J. Virol. *76*, 791–801.

48. Grieger, J.C., Choi, V.W., and Samulski, R.J. (2006). Production and characterization of adeno-associated viral vectors. Nat. Protoc. *1*, 1412–1428.

49. Clark, K.R., Liu, X., McGrath, J.P., and Johnson, P.R. (1999). Highly purified recombinant adeno-associated virus vectors are biologically active and free of detectable helper and wild-type viruses. Hum. Gene Ther. *10*, 1031–1039.

50. Rafael-Fortney, J.A., Chimanji, N.S., Schill, K.E., Martin, C.D., Murray, J.D., Ganguly, R., Stangland, J.E., Tran, T., Xu, Y., Canan, B.D., et al. (2011). Early treatment with lisinopril and spironolactone preserves cardiac and skeletal muscle in Duchenne muscular dystrophy mice. Circulation *124*, 582–588.

51. Moorwood, C., Liu, M., Tian, Z., and Barton, E. (2013). Isometric and Eccentric Force Generation Assessment of Skeletal Muscles Isolated from Murine Models of Muscular Dystrophies. J. Vis. Exp. *71*, e50036.

52. Võikar, V., Polus, A., Vasar, E., and Rauvala, H. (2005). Long-term individual housing in C57BL/6J and DBA/2 mice: assessment of behavioral consequences. Genes Brain Behav. *4*, 240–252.